Local concentration profile of colloidal particles inside a charged cylindrical pore

M. Chávez-Páez,[1] H. Acuña-Campa,[2] L. Yeomans-Reyna,[2] M. Valdez-Covarrubias,[2] and M. Medina-Noyola[1]
[1]*Instituto de Física ''Manuel Sandoval Vallarta,'' Universidad Autónoma de San Luis Potosí, Apartado Postal 629, 78000 San Luis Potosí, S.L.P., México*
[2]*Departamento de Física, Universidad de Sonora, Apartado Postal 1626, 83000 Hermosillo Sonora, México*
(Received 6 September 1996)

A simple theoretical scheme is employed to calculate the equilibrium local concentration profile of a model suspension of highly charged colloidal particles inside a cylindrical pore in the regime corresponding to thick and narrow pores. In addition, we report results of Brownian dynamics simulations for some of the systems presented here. We have found that the local concentration profile in this geometry scales in quite a similar way as in the vicinity of a confining charged wall. [S1063-651X(97)01204-X]

PACS number(s): 82.70.Dd, 05.40.+j

I. INTRODUCTION

The properties of liquids confined in restricted spaces has been the subject of long-standing theoretical and practical interest [1]. Understanding how the equilibrium structure and transport properties of confined liquids compare to their bulk properties is an important issue in many practical processes and systems, such as those involving a liquid that permeates a porous medium [2]. One interesting regime is that in which the relevant scale of the confining geometry (e.g., the size of the pores) is of the order of the mean interparticle distance. At this space scale, a molecular description of the properties of the fluid cannot be avoided. Although the observation of the average structure of the few molecules of a liquid that permeates a very narrow pore may not be easy to observe in truly molecular systems, similar conditions may appear or may be prepared at a mesoscopic scale in the field of colloid physics. Thus, for example, the colloidal realization of a fluid confined between two parallel walls has been observed rather directly by video microscopy techniques [3]. As the distance between the confining walls increases, the evolution of the main structural features of the system is followed, as the confinement varies from the extreme condition corresponding to a quasi-two-dimensional liquid or crystal, through the destabilization of the corresponding monolayer, up to the appearance of a three-dimensional (3D) bulk region between the plates [3]. These experiments have stimulated the corresponding theoretical work, one aspect of which demands the methods of the statistical mechanical theory of inhomogeneous fluids [4]. Although the precise determination of the effective forces between the colloidal particles of the confined suspension must be the subject of careful study [5], it is also true that some of the most general structural properties may depend on rather general features of these effective interactions. Thus, it is also instructive to study the properties of somewhat idealized models based on some simple and general types of effective pair forces. For example, in recent work, the structure of a Yukawa fluid confined by two parallel walls was studied theoretically, and by computer simulations [6]. In addition to the general and rather expected features of the local structure induced by the confinement, other interesting effects were also revealed by these studies, such as the possibility of the formation of an adsorbed monolayer at the confining walls, and the formation of a depletion gap in the neighborhood of such a monolayer [7]. Similarly, in the context of the study of simple fluids inside cylindrical pores, interesting layering transitions have also been predicted [8].

Very much along this line of research, in this paper we report the results of our recent work on the description of a model colloidal fluid (the Yukawa fluid) that permeates a narrow cylindrical pore. Here we calculate the local concentration $n(\mathbf{r})$ of fluid particles in the interior of the pore, which are in contact with a reservoir at bulk concentration n. The theoretical calculations derive from a simple approximate scheme, based on the Wertheim-Lovett equation for $n(\mathbf{r})$ complemented with the so-called hypernetted chain (HNC) closure plus the simplification that replaces the inhomogeneous two-particle direct correlation function by its bulk value [9]. This approximate theory allows us to calculate the local concentration profile $n(\mathbf{r})$ for a variety of conditions. In order to assess the accuracy of these predictions, we perform Brownian dynamics computer simulations, which are also reported. The comparison indicates that the approximate theoretical scheme does provide the correct general picture of this structural property, although the quantitative comparison is very similar to what was observed for the Yukawa fluid permeating the space between two parallel walls [9]. In Sec. II we explain the model system studied, the approximate theory employed to calculate $n(\mathbf{r})$, and give some details of the computer simulations. The results are presented and discussed in Sec. III. The main conclusions are summarized in Sec. IV.

II. MODEL SYSTEM AND APPROXIMATE THEORY

To illustrate the general experimental conditions that we have in mind, consider a colloidal suspension of highly charged polystyrene spheres in water at low ionic strength. Imagine that we have a very long capillary of conical shape of length L and internal radius R_M and R_m at its two extremes, with $R_M > R_m$, and $L \gg R_M$. If immersed in the suspension, and after equilibrium is reached, the colloidal particles will penetrate the interior of the capillary. We then ask what is the local structure (i.e., the average local concentration) of the suspended particles at any point in the interior of

this capillary, for given elementary parameters such as those pertaining to the suspension (the diameter σ, charge Q, the bulk concentration of the colloidal particles, and the inverse Debye length κ), and those referring to the capillary (the length L and radii R_M and R_m, and the internal surface charge density σ_{el}). Rather than stressing the many complications involved in preparing and characterizing this system (i.e., in determining those parameters), we consider instead an idealized and simplified limiting model. Thus, we shall only consider the limit in which the capillary looks locally cylindrical, and will study the structure of the colloidal fluid inside an infinitely long cylinder of radius R. In this limit, $n(\mathbf{r})=n(\rho;R)$, where ρ is the distance from the cylinder's axis.

As for the potential $\Psi(\mathbf{r})$ of the force exerted by the charge density of the cylinder's inner surface, on a particle of charge Q at position $\mathbf{r}$ inside the cylinder, we shall introduce some simplifications on top of the conventional Debye-Hückel approximation [10,11]. Thus, we assume that $\Psi(\mathbf{r})$ is given by $\Psi(\mathbf{r})=Q\psi(\mathbf{r})$, where $\psi(\mathbf{r})$ is the solution of the linearized Poisson-Boltzmann equation $\nabla^2\psi(\mathbf{r})=\kappa^2\psi(\mathbf{r})$ for $\mathbf{r}$ inside the capillary, where κ is the inverse Debye length. Solving this equation with the adequate boundary conditions, one finds that, for an infinitely long cylinder, $\Psi(\rho)$ can be written as

$$\beta\Psi(\rho)=\alpha I_0(\kappa\rho), \tag{2.1}$$

where $\beta=(k_BT)^{-1}$, with k_B being Boltzmann's constant and T the temperature, and where $I_0(x)$ is the modified Bessel function of order zero [12]. In this equation, α is a constant that depends on R and is linear in Q and in σ. We find it more convenient to rewrite this equation as

$$\beta\Psi(\rho)=K_w\frac{I_0(\kappa\rho)}{I_0(\kappa R')-1}, \quad \rho<R', \tag{2.2}$$

with R' being the distance from the cylinder axis to the point at which a particle is in contact with the cylinder's inner hard wall. Thus, if R is the actual radius of the cylinder, and if we assume the particle to have a hard-sphere diameter σ, then $R'\equiv R-\sigma/2$, and K_w is the electrostatic potential energy, in units of k_BT, of a particle in contact with the cylinder wall, referred to the potential at the center of the cylinder.

Concerning the pair potential between two colloidal particles, it will be modeled by the screened Coulomb or Yukawa potential [10,13]. This is, of course, completely justified when the two particles are in the bulk suspension, but when they are in the interior of a very narrow pore, the conditions of confinement will definitely give rise to modifications from this simple pair potential. Nevertheless, one can expect that the Yukawa form is still a reasonable zeroth order approximation, which at least retains the basic soft repulsive character that a more detailed calculation is expected to exhibit. To conform with previous work of a similar kind [9], we write the pair potential in dimensionless form as

$$\beta u(r)=\begin{cases}\infty, & r<\sigma\\ \dfrac{K\exp[-z(r/\sigma-1)]}{(r/\sigma)}, & r>\sigma,\end{cases} \tag{2.3}$$

where $z\equiv\kappa\sigma$.

Once we have specified the one- and two-particle potentials, the next step is to define the approximate theoretical scheme that allows us to calculate $n(\rho)$. Just as in Ref. [9], our theoretical calculations will also be based on the Wertheim-Lovett equation of the theory of inhomogeneous fluids, which, complemented with the HNC closure [4], reads

$$\ln n(\mathbf{r})+\beta\Psi(\mathbf{r})-\int d^3r'\,c_b(|\mathbf{r}-\mathbf{r}'|)n(\mathbf{r}')=\text{const}, \tag{2.4}$$

where the additional simplification, consisting of the replacement of the inhomogeneous direct correlation function $c(\mathbf{r},\mathbf{r}')$ by its bulk value $c_b(|\mathbf{r}-\mathbf{r}'|)$, was also introduced. The constant on the right-hand side of this equation is eliminated by subtracting the same equation evaluated at a point in the bulk, where $n(\mathbf{r})=n$ and $\Psi(\mathbf{r})=0$. Thus, defining the function $H(\mathbf{r})$ by means of the relation

$$n(\mathbf{r})\equiv n[1+H(\mathbf{r})], \tag{2.5}$$

and recognizing the fact that $\Psi(\mathbf{r})$, and hence also $H(\mathbf{r})$, only depends on the radial distance ρ to the cylinder's axis, we can rewrite Eq. (2.4) as

$$\ln[1+H(\rho)]+\beta\Psi(\rho)-n\int d^3r'\,c_b(|\mathbf{r}-\mathbf{r}'|)H(\rho')=0. \tag{2.6}$$

This is a nonlinear equation that has to be solved numerically. Here we have implemented the method described by Zhou and Stell [14], which writes this equation in terms of the direct and inverse Fourier transform of the functions involved. The bulk direct correlation function $c_b(r)$ was obtained by solving the Ornstein-Zernike equation in the bulk, using the Rogers-Young closure relation [15].

To assess the predictions of our simplified model, we have carried out Brownian dynamics simulations to calculate the concentration profile of the particles confined inside the cylinder. The method of Brownian dynamics, as proposed by Ermak and McCammon [16], is based on the solution of the generalized N-particle diffusion equation. Within this scheme, the displacement of the ith particle (during a short enough time interval Δt) is given by

$$\mathbf{r}_i(t+\Delta t)-\mathbf{r}_i(t)=\beta D_0\mathbf{F}_i\Delta t+\mathbf{R}_i(\Delta t), \tag{2.7}$$

where D_0 is the free-particle diffusion coefficient, and $\mathbf{R}_i(\Delta t)$ is a random Gaussian displacement of the particle, which is assumed to have zero mean and variance $6D_0\Delta t$. The force $\mathbf{F}_i$ in this equation arises from the direct interactions of the ith particle with the cylinder's field of force and with the other Brownian particles in the system. Also, in order to minimize edge effects due to the finite size of the simulation system, we have used conventional [17] periodic boundary conditions in the z direction.

The connection of the computer simulations with the theoretical results is made by fixing the total number of particles N inside the volume πR^2L of the basic simulation cell (of length L in the z direction) such that

$$n_{\mathrm{av}} \equiv \frac{N}{\pi R^2 L} = \frac{\int_0^R n[1+H(\rho)]2\pi\rho d\rho}{\pi R^2}, \qquad (2.8)$$

where $H(\rho)$ is obtained from the solution of Eq. (2.6). In practice, for a given system (i.e., fixed one- and two-particle interaction potentials, and fixed n), Eq. (2.8) fixes the ratio N/L. Thus, we made the pertinent tests to discard any dependence of the simulation results on N and/or on L by varying these parameters, keeping their ratio fixed by Eq. (2.8), until no dependence was found on $H(\rho)$. In many cases we found that already with $N \sim 100$ convergence was observed, particularly when the ratio N/L was small.

III. RESULTS

Let us now present the results for $n^*(\rho) \equiv n^*[1+H(\rho)]$, where n^* is the dimensionless bulk number concentration $n^* = n\sigma^3$. For a systematic presentation of our results, let us notice that the independent parameters that we could vary are those referring to the bulk suspension, namely, the Yukawa parameters K and z, and the bulk concentration n^*, and the parameters referring to the wall-particle interaction, namely, K_w and R'. Varying those five parameters we can generate all the possible structures that the Yukawa fluid will adopt when confined in the interior of the cylinder. Here we shall not exhaust all those possible structures, but will choose some of them to illustrate the various regimes that appear when the screened electrostatic interactions dominate. Thus, for concreteness, let us consider a typical suspension of highly charged spheres at low ionic strength. Parameters representative of these conditions are $z=0.15$, $K=400$, and $n^*=8.4\times10^{-4}$. One relevant length for this system is the mean interparticle distance $\ell^* = \ell/\sigma \equiv n^{*-1/3}$, which for this system is about $\ell^* = 10.6$, i.e., of the order of the screening length z^{-1} ($=6.67$ for this system). The bulk structure for this system is represented by the radial distribution function $g(r)$, which defines another relevant length scale, namely, the correlation length λ (the distance at which $g(r)$ reaches its asymptotic limit). For the particular suspension that we are using as an illustration, $\lambda^* = \lambda/\sigma \sim 5\ell^*$.

Let us now consider the structure of the suspension inside a cylinder of radius R' and repulsion parameter K_w, in contact with the bulk reservoir above. In first approximation we can classify the various possible structures inside the cylinder in terms of the ratio of the mean interparticle distance ℓ and the radius R'. In reality, we shall restrict ourselves to values of K_w large enough so that the hard contact between one particle and the wall will be completely unlikely. Thus, $n(\rho)$ will always be nearly zero not only at contact, but also within a finite region between the wall ($\rho = R'$) and a certain effective distance d of closest approach to the wall. This defines an effective radius $R_{\mathrm{ef}} = R' - d$ of the cylinder, which will depend on R' but also on K_w. Thus, if we compare ℓ with the thickness of the cylinder, it makes more sense to compare ℓ with R_{ef}, rather than with R' itself.

A. Very thick cylinders

Let us first consider ''very thick'' cylinders, i.e., the regime in which $R_{\mathrm{ef}} \gg \ell$. First of all, let us notice that in the actual limit $\ell/R' \to 0$, the structure of the confined Yukawa fluid inside a cylinder approaches that of the same fluid near a charged planar wall, a condition studied previously. The solid line in Fig. 1 exhibits $n(\rho)$ as a function of $x \equiv R' - \rho$, as obtained from the solution of our theory, for the illustrative bulk parameters above ($K=400$, $z=0.15$, $n^*=8.4\times10^{-4}$), and for $K_w=400$ and $R'=100\sigma$. As it turns out, already for this radius, the shape of $n(\rho)$ near the wall has approached its asymptotic value corresponding to a flat surface ($R'=\infty$), up to the resolution of the figure. From the solid line, we can see that the distance of closest approach to the wall is about $d^* \approx 10$, so that the effective radius corresponding to $K_w=400$ and $R'=100\sigma$ is about $R_{\mathrm{ef}} \approx 90\sigma$. The other important feature to notice is that R_{ef} is not only much larger than ℓ ($\approx 10.6\sigma$), but is already larger than the bulk correlation length λ ($\approx 50\sigma$). As a result, the local concentration $n^*(\rho)$ attains its bulk value n^* inside a region around the cylinder axis, defined approximately as $\rho < (R_{\mathrm{ef}} - \lambda)$. Thus, we can say that the solid line in Fig. 1, which corresponds to a thick cylinder of large but finite radius, is representative of the regime in which the structure of the confined Yukawa fluid is virtually identical to the structure of the fluid near a flat wall, and with a well-defined bulk region in the middle of the cylinder.

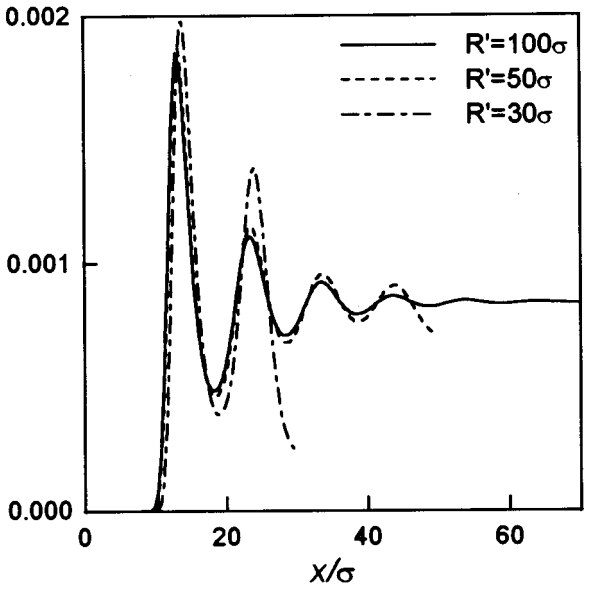

FIG. 1. Local concentration profile $n^*(\rho)$, plotted as a function of $x = R' - \rho$, for three different values of R' ($R' = 30\sigma$, 50σ, 100σ) and for $K_w = 400$. The bulk parameters are $n^* = 8.4\times10^{-4}$, $K=400$, and $z=0.15$.

In this regime, two interesting scaling properties are observed in $n(\rho)$. The first of them refers to the fact that $n(\rho)$ only depends on the bulk parameters n^*, K, and z, and on K_w, but not on R', when $n(\rho)$ is plotted as a function of the wall-particle distance $x = R' - \rho$, as done in Fig. 1. Thus, the solid line in that figure not only corresponds to $R' = 100\sigma$, but also to any other value of R' larger than 100σ, as well as to values of R' smaller than 100σ, but still larger than λ ($\approx 50\sigma$), say, down to about $R' \approx 70\sigma$. For R' of the order of λ, deviations from this rule are observed. This is illustrated in Fig. 1 by the curve, corresponding to

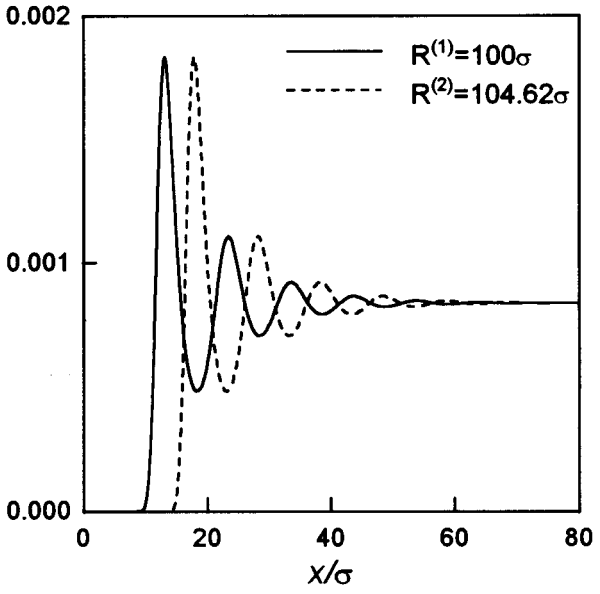

FIG. 2. Local concentration profile $n^*(\rho)$, plotted as a function of $x=R'-\rho$, for two different values of K_w and R'. The solid line corresponds to $K_w=400$ and $R'=R^{(1)}=100\sigma$. The dashed line corresponds to $K_w=800$ and $R'=R^{(2)}=104.62\sigma$. The bulk parameters are the same as in the previous figure.

$R'=50\sigma$, which is slightly below the threshold condition $R_{\rm ef}\approx\lambda$. As one can see from the comparison with the solid line ($R'=100\sigma$), the quantitative differences are still rather small, even though for $R'=50\sigma$ the bulk region around the cylinder axis has disappeared completely. It is also interesting to notice that even if we decrease R' still further, so that the structure of $n(R'-x)$ is constituted only by two maxima, at least the shape and position of the main peak are still not dramatically different from the limiting condition $R'\to\infty$. This is also illustrated in Fig. 1 by the curve corresponding to $R'=30\sigma$, in which $R_{\rm ef}\approx 20\sigma$, i.e., only twice ℓ, and definitely smaller than the correlation length λ.

The fact that $n(R'-x)$ becomes independent of R' for large cylinder radius should not be surprising. The reason is that the wall-particle potential $\Psi(\rho)$ in Eq. (2.2), which in general depends on K_w and R', becomes independent of R' for large R' when written in terms of the wall-particle distance x, i.e., when $R'\to\infty$, $\beta\Psi(R'-x)\approx K_w e^{-\kappa x}$. In this very same limit, and for the same reason, a second scaling property of $n(R'-x)$ can be predicted. Thus, notice that the asymptotic form (large R') of the wall-particle potential, $\beta\Psi(\rho,R',K_w)=K_w e^{-\kappa(R'-\rho)}$, has the property

$$\beta\Psi(\rho,R^{(1)},K_w^{(1)})=\beta\Psi(\rho,R^{(2)},K_w^{(2)}), \tag{3.1}$$

provided that $R^{(2)}=R^{(1)}+\delta$, with $\delta=\kappa^{-1}\ln(K_w^{(2)}/K_w^{(1)})$. This means that the force that a particle feels at a distance ρ from the axis of a cylinder radius $R^{(1)}$ and wall-particle parameter $K_w^{(1)}$ is the same as that felt by the same particle at the same distance from the axis of another cylinder of radius $R^{(2)}$ and wall-particle parameter $K_w^{(2)}$, provided that $R^{(2)}=R^{(1)}+\kappa^{-1}\ln(K_w^{(2)}/K_w^{(1)})$. As a consequence, the particles from the same reservoir will structure identically [when $n(\rho)$ is plotted as a function of ρ] when they penetrate these

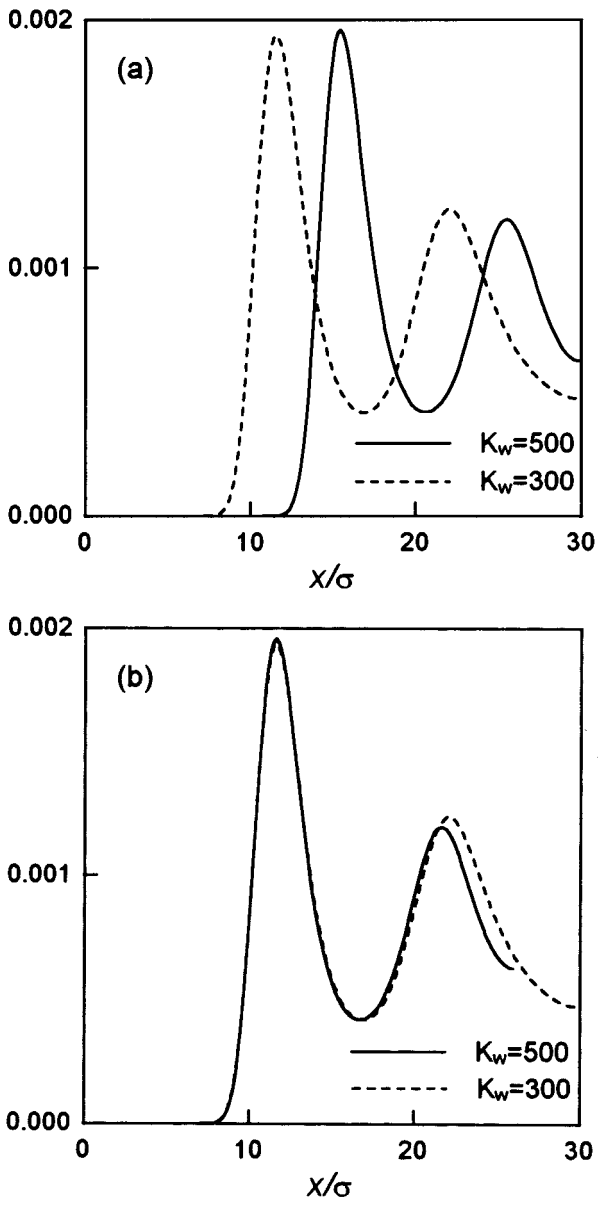

FIG. 3. Local concentration profile $n^*(\rho)$, plotted as a function of $x=R'-\rho$, for $R'=30\sigma$, and $K_w=300$, and $K_w=500$, and for the same bulk parameters as in Fig. 1. In (b) we have shifted the curve corresponding to $K_w=500$ to the left by $\delta=\kappa^{-1}\ln(K_w^{(2)}/K_w^{(1)})=4.62\sigma$.

two cylinders. Clearly, when $n(\rho)$ is plotted as a function of the wall-particle distance $x=R'-\rho$, the two curves will appear shifted by a displacement given by $\delta=\kappa^{-1}\ln(K_w^{(2)}/K_w^{(1)})$. This is illustrated in Fig. 2, where $n(R'-x;K_w)$ is plotted for the same bulk conditions as in Fig. 1 for two different cylinder parameters, namely, $K_w^{(1)}=400$, $R^{(1)}=100\sigma$ (solid line), $K_w^{(2)}=800$, and $R^{(2)}=104.62\sigma$ (dashed line), which satisfy $R^{(2)}=R^{(1)}+\kappa^{-1}\ln(K_w^{(2)}/K_w^{(1)})$. If we displace the second curve to the left by $\delta=4.62\sigma$, it coincides exactly with the solid curve.

We can summarize the consequences of the two scaling properties of $n(\rho)$ by the following statement. In the region of thick cylinders, when a well-defined bulk region is observed in the middle of the cylinder, the shape of $n(\rho,R',K_w)$ does not depend on R' when plotted as a func-

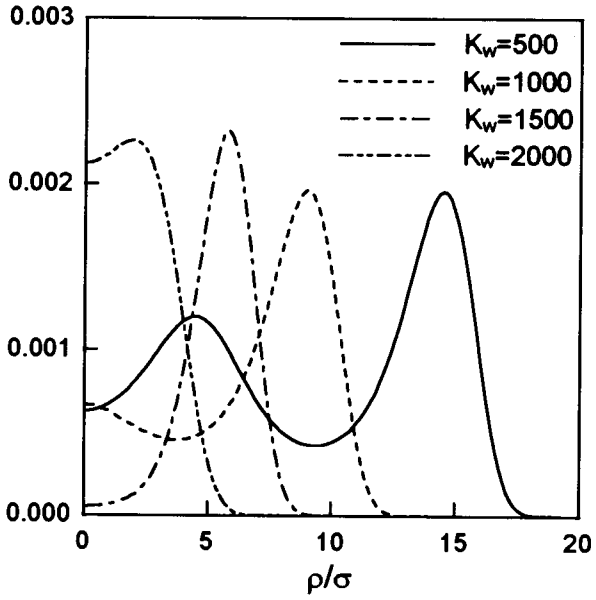

FIG. 4. Local concentration profile $n^*(\rho)$ for $R'=30\sigma$ and for $K_w=500$, 1000, 1500, and 2000. The bulk parameters are the same as in Fig. 1.

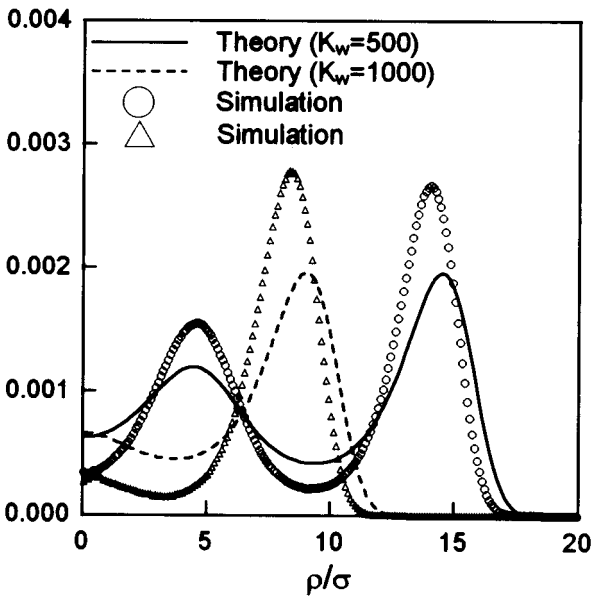

FIG. 5. Comparison between the theoretical results for $n^*(\rho)$ (lines) and computer simulations (symbols), for $R'=30\sigma$, and for $K_w=500$ and 1000. Open circles correspond to simulation results with $K_w=500$. Open triangles correspond to simulations with $K_w=1000$. The bulk parameters are the same as in Fig. 1.

tion of the wall-particle distance $x=R'-\rho$. Furthermore, it is also independent of K_w, since any two curves $n(x)$ corresponding to two different values of K_w will superimpose after shifting one curve towards the other by a displacement of the coordinate x given by $\delta=\kappa^{-1}\ln(K_w^{(2)}/K_w^{(1)})$.

B. Narrow Cylinders

Let us now discuss the regime in which $R_{\rm ef}\approx\ell$. Already in Fig. 1 we presented the results for $R'=30\sigma$, $K_w=400$ in the context of our discussion on the dependence of $n(\rho)$ on the cylinder's radius R'. There we saw that the scaling property valid for thick cylinders, and consisting of the independence of $n(R'-x)$ on R', broke down for $R'=30\sigma$, well inside the regime that we are now discussing ($R_{\rm ef}\approx\ell$), although the shape and position of the main peak of $n(R'-x)$ were clearly reminiscent of the limiting structure for large R'. In Fig. 3(a) we now illustrate the consequences of increasing K_w from $K_w=300$ to $K_w=500$, for the same reservoir as in Figs. 1 and 2, but for a relatively narrow cylinder ($R'=30\sigma$). An obvious question here is to what extent the second scaling property will still apply in this regime (well outside the regime of very thick cylinders). As indicated in Fig. 3(b), after shifting the solid curve until the two maxima are in the same position, and as expected, the two curves do not coincide exactly, but they are remarkably similar, even quantitatively. Besides this observation, Fig. 3(a) also illustrates the main features of the evolution of $n(\rho)$ when K_w increases, keeping R' fixed, namely, the shifting of the main peak of $n(\rho)$ away from the wall, and the approach of the second peak towards the cylinder's axis.

In Fig. 4 we plot $n(\rho)$, now as a function of the distance from the axis, for $K_w=500$, 1000, 1500, and 2000, to illustrate the eventual disappearing of the second peak, and the corresponding approach of the main peak to the cylinder's axis. In this sequence, the radius of the cylinder was kept fixed ($R'=30\sigma$). We should mention that a similar trend is observed if we keep K_w fixed, while decreasing R'. In either case one interesting structure is observed, illustrated in Fig. 4 by the curve corresponding to $K_w=1500$. This is characterized by a single, fairly well defined peak in $n(\rho)$, of width $\Delta\rho$, located at a distance $\rho_{\rm max}$ from the axis. For this particular case, $\Delta\rho\approx4\sigma$, and $\rho_{\rm max}\approx6\sigma$. Thus, $(\Delta\rho/2)<\rho_{\rm max}$, and this means that for this value of K_w, the region inside the cylinder of radius R' to which the particles are confined is a cylindrical shell of inner radius $\rho_{\rm max}-\Delta\rho/2$, and outer radius $\rho_{\rm max}+\Delta\rho/2$. This is a remarkable condition of self-confinement resulting from the equilibrium of the wall-particle interactions, which tend to confine all the particles at the cylinder axis, and the particle-particle repulsions, which tend to expand the volume occupied by the particles. Clearly, if the wall-particle interactions continue to increase, as indicated by the curve corresponding to $K_w=2000$, the position of the peak is shifted towards the axis, resulting eventually in a single peak located at $\rho_{\rm max}=0$. Further increase in K_w will result in the eventual expulsion of all the particles inside the cylinder, manifested in a decrease of the height of the remaining central peak of $n(\rho)$.

C. Comparison with computer simulations

In this manner, we have described the sequence of structural changes in $n(\rho)$ predicted by the theory, when the wall-particle parameters R' and K_w are varied, keeping the bulk parameters n^*, z, and K fixed. The general conclusion is that the main qualitative effects are basically the same if we either decrease R' or increase K_w. These effects refer to a progressive confining of the particles toward the center, and their eventual expulsion from the cylinder. Let us now comment on the results of the computer simulations for the same property. The most interesting regime in our analysis is that in which the effective radius $R_{\rm ef}$ is of the order of the corre-

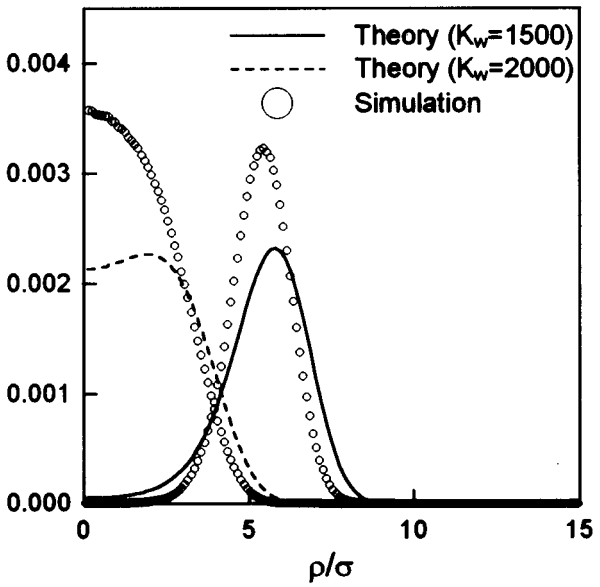

FIG. 6. Same as in Fig. 5, but with $K_w = 1500$ and 2000.

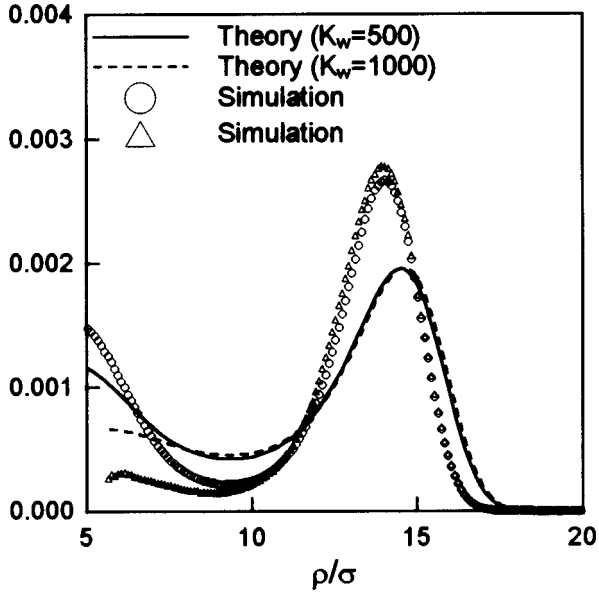

FIG. 7. Same results as in Fig. 5, but with the theoretical and simulated data corresponding to $K_w = 1000$ shifted to the right by $\delta = 5.6\sigma$.

lation length, or even of the mean distance. This regime was illustrated here by Figs. 3 and 4. Before presenting the corresponding simulation results, let us mention that the comparison between the present theory and the computer simulation was already discussed in the context of the planar geometry [9]. Such discussion applies to our present problem when we refer to the regime of very thick cylinders ($R' \to \infty$; see Fig. 1). As illustrated in [9], the computer simulations exhibit the same general features predicted by the theory, and except for quantitative discrepancies in the heights of the maxima and minima of $n(R'-x)$, the general quantitative agreement between theory and simulations can be said to be good. Although with a little less quantitative accuracy, the same statement can be made concerning the corresponding comparison (theory versus simulations) in the interior of narrow cylinders, and this is what we now discuss.

In Figs. 5 and 6 we have again the four curves of Fig. 4, but now compared with their corresponding computer simulation results. These figures illustrate the nature of the general agreement between the present theory and the corresponding simulations. From this comparison, we find that the agreement is qualitatively pretty good, concerning the number and location of the maxima of $n(\rho)$. Their height, however, is generally underestimated by the theoretical predictions. These comments apply to most of the conditions we studied, including those employed here to illustrate them. The most important departures refer to the most extreme case illustrated by the curve corresponding to $K_w = 2000$ in Fig. 6, in which the structure of $n(\rho)$ is reduced to a single peak, almost centered at the axis. It is also interesting to notice that the scaling properties discussed before continue to hold, although in an approximate manner, even in the regime illustrated by Fig. 5, which is well outside the regime corresponding to thick cylinders. Thus, as discussed above for large R', the shape of $n(\rho)$ does not depend on R' or K_w, thus being a function only of the bulk parameters n^*, z, and K, provided the curves for $n(\rho)$ for different R' and K_w are made to coincide in the position, for example, of the first maximum. This is illustrated in Fig. 7, where the curves corresponding to $K_w = 1000$ were shifted so that the position of the main peak of the computer simulated $n(\rho)$ coincides with the position of the main peak of the computer simulated $n(\rho)$ corresponding to $K_w = 500$. The magnitude of the displacement δ, however, is no longer explained by the rule $\delta = \kappa^{-1}\ln(K_w^{(2)}/K_w^{(1)})$, which holds for thick cylinders (this rule would predict $\delta = 4.62\sigma$, whereas the displacement needed for Fig. 7 was $\delta \approx 5.6\sigma$). As observed from this figure, however, the scaling rule holds here to a very good degree of quantitative accuracy, both for the theoretical and the simulated results, at least regarding the main peak of $n(\rho)$.

IV. CONCLUSIONS

We can now summarize the results presented in this paper. First of all, we learned the scaling properties of $n(\rho)$, which basically states that the independence of $n(\rho)$ on the wall-particle interaction parameters R' and K_w, when plotted adequately, holds quite accurately for thick cylinders. Surprisingly enough, however, the same prediction holds semiquantitatively also for very narrow cylinders. Our discussion was illustrated with both theoretical calculations and computer simulations for a typical bulk system ($n^* = 8.4\times10^{-4}$, $z = 0.15$, $K = 400$), varying the wall-particle parameters R' and K_w. The same scenario, however, was observed when n^* was varied. In fact, increasing n^* leads to similar effects as increasing K. In both cases this leads to an increase of the effects of the interparticle Yukawa repulsions, manifested by a more pronounced structure in $n(\rho)$ (i.e., higher maxima and lower minima), and by a reduction of the effective distance of closest approach of the particles to the cylinder hard wall.

All the conclusions above are only valid as long as we restrict ourselves to systems in which direct hard-core contact between two particles and between one particle and the cylinder hard wall are prevented by a large value of both K

and K_w, respectively. When these conditions are not met, at least in the asymptotic limit $R' \to \infty$, one should expect other interesting effects, such as the formation of an adsorbed monolayer in contact with the cylinder wall, followed by a depletion layer where the particles are not allowed to be in. As we have seen in the last figures here, however, already in the regime studied here other interesting effects appear, such as the confinement of the particles to a cylindrical shell of width $\Delta\rho$, and position $\rho_{\max}$, which collapses to a single central peak in $n(\rho)$ when the confining is extreme. In this extreme limit, the particles are virtually confined to the cylinder axis, with small radial deviations of extent $\Delta\rho$. The opposite process, in which this axial string of particles is destabilized, corresponds to the buckling transition. This corresponds to the condition in which the system breaks its confinement to essentially one dimension, to form structures that use the radial dimension made available when K_w is reduced or R' is increased. Unfortunately, the most interesting features of this transition are not captures by the theoretical approach employed here, although some of them are neatly revealed by the computer simulations. The discussion of this aspect, along with others that fall outside the scope of this paper, is currently being investigated in detail.

ACKNOWLEDGMENTS

The authors wish to thank Dr. J. M. Méndez-Alcaraz for providing the program to calculate the Rogers-Young's bulk direct correlation function. We also thank the Computer Center of the Universidad de Guadalajara, México, where some calculations were performed. This work was partially supported by the Consejo Nacional de Ciencia y Tecnología (CONACyT, México) through Grant No. 2882E.

[1] M. Lozada-Cassou (revision article), *Fundamentals of Inhomogeneous Fluids*. edited by D. Henderson (Marcel Dekker, New York, 1992).
[2] M. Sahimi, Rev. Mod. Phys. **65**, 1393 (1993).
[3] D. H. van Winkle and C. A. Murray, J. Chem. Phys. **89**, 2885 (1988).
[4] R. Evans, Adv. Phys. **28**, 143 (1979).
[5] M. D. Carbajal-Tinoco, F. Castro-Román, and J. L. Arauz-Lara, Phys. Rev. E **53**, 3745 (1996); G. M. Kepler and S. Fraden, Phys. Rev. Lett. **73**, 356 (1994); J. C. Crocker and D. G. Grier, *ibid.* **73**, 352 (1994).
[6] (a) P. González-Mozuelos, J. Chem. Phys. **98**, 5747 (1993); (b) P. González-Mozuelos and J. Alejandre, J. Chem. Phys. **105**, 5949 (1996).
[7] P. González-Mozuelos, J. Alejandre, and M. Medina-Noyola, J. Chem. Phys. **97**, 8712 (1992).
[8] B. K. Peterson, G. S. Heffelfinger, K. E. Gubbins, and F. van Swol, J. Chem. Phys. **93**, 679 (1990).
[9] P. González-Mozuelos, J. Alejandre, and M. Medina-Noyola, J. Chem. Phys. **95**, 8337 (1991).
[10] E. J. W. Verwey and J. T. G. Overbeek, *Theory of the Stability of Lyophobic Colloids* (Elsevier, Amsterdam, 1948).
[11] D. A. McQuarrie, *Statistical Mechanics* (Harper and Row, New York, 1975).
[12] G. Arfken, *Métodos Matemáticos para Físicos* (Editorial DIANA, México, 1981).
[13] M. Medina-Noyola and D. A. McQuarrie, J. Chem. Phys. **73**, 6279 (1980).
[14] Y. Zhou and G. Stell, Mol. Phys. **66**, 791 (1989).
[15] F. J. Rogers and D. A. Young, Phys. Rev. A **30**, 999 (1984).
[16] D. L. Ermak and J. A. McCammon, J. Chem. Phys. **64**, 1352 (1978).
[17] M. P. Allen and D. J. Tildesley, *Computer Simulation of Liquids* (Oxford Science, New York, 1987).